International Journal of Nanomedicine

Dovepress
open access to scientific and medical research

Open Access Full Text Article

ORIGINAL RESEARCH

Hypoxia and Singlet Oxygen Dual-Responsive Micelles for Photodynamic and Chemotherapy Therapy Featured with Enhanced Cellular Uptake and Triggered Cargo Delivery

Xuliang Guo, Lefei Han, Wenyu Chen, Huixin He, Weijin Zhang, Chaoqi Huang, Xiu Wang

School of Pharmacy, Bengbu Medical College, Bengbu, Anhui, People's Republic of China

Correspondence: Xiu Wang; Xuliang Guo, Department of Pharmacy, Bengbu Medical College, No. 2600 Donghai Road, Bengbu, People's Republic of China, Email bbwx1016@163.com; 2021001@bbmc.edu.cn

Introduction: Combination therapy provides better outcomes than a single therapy and becomes an efficient strategy for cancer treatment. In this study, we designed a hypoxia- and singlet oxygen-responsive polymeric micelles which contain azo and nitroimidazole groups for enhanced cellular uptake, repaid cargo release, and codelivery of photosensitizer Ce6 and hypoxia-activated prodrug tirapazamine TPZ (DHM-Ce6@TPZ), which could be used for combining Ce6-mediated photodynamic therapy (PDT) and PDT-activated chemotherapy to enhance the therapy effect of cancer.

Methods: The hypoxia- and singlet oxygen-responsive polymeric micelles DHM-Ce6@TPZ were prepared by film hydration method. The morphology, physicochemical properties, stimuli responsiveness, in vitro singlet oxygen production, cellular uptake, and cell viability were evaluated. In addition, the in vivo therapeutic effects of the micelles were verified using a tumor xenograft mice model.

Results: The resulting dual-responsive micelles not only increased the concentration of intracellular photosensitizer and TPZ, but also facilitated photosensitizer and TPZ release for enhanced integration of photodynamic and chemotherapy therapy. As a photosensitizer, Ce6 induced PDT by generating toxic singlet reactive oxygen species (ROS), resulting in a hypoxic tumor environment to activate the prodrug TPZ to achieve efficient chemotherapy, thereby evoking a synergistic photodynamic and chemotherapy therapeutic effect. The cascade synergistic therapeutic effect of DHM-Ce6@TPZ was effectively evaluated both in vitro and in vivo to inhibit tumor growth in a breast cancer mice model.

Conclusion: The designed multifunctional micellar nano platform could be a convenient and powerful vehicle for the efficient co-delivery of photosensitizers and chemical drugs for enhanced synergistic photodynamic and chemotherapy therapeutic effect of cancer.

Keywords: photodynamic therapy, hypoxia-responsive, singlet oxygen-responsive, combination therapy

Introduction

Cancer is one of the major diseases that harm human health.[1–3] The traditional methods of surgery, chemotherapy, and radiotherapy have many problems in the treatment of cancer, such as limited efficacy and inescapable side effects.[4] In recent years, some new treatment means such as photothermal therapy (PTT) and photodynamic therapy (PDT) has broadened the field of anti-cancer therapy.[5,6] PDT is a new non-invasive tumor treatment method triggered by external light, which has the advantages of low trauma, low toxicity, great selectivity, and good controllability.[6–8] Photosensitizers, oxygen, and light are the three factors of anti-tumor PDT, for which the photosensitizers were excited by light irradiation, and oxygen molecules generated reactive oxygen species (ROS) through energy transmission, resulting in damage and even death of tumor cells.[9–12] The therapeutic efficiency of PDT is highly dependent on oxygen content in tumors, cellular internalization of nanocarriers, and on-demand release of photosensitizers in tumor tissues.[6] However, because of the aberrant tissue structure and lack of

Received: 26 July 2023
Accepted: 13 December 2023
Published: 12 January 2024

blood vessels, the oxygen content of tumor cells is not uniform, which severely astricts the anti-tumor effect of PDT in relatively hypoxic areas.[13] Many studies have focused on exogenous oxygen delivery or endogenous catalytic oxygen production to increase oxygen concentration in tumor tissues and thus enhance the PDT effect.[14–16] Since the consumption of oxygen will aggravate the degree of hypoxia at the tumor site, another method can be put forward through reverse thinking, that is, using the hypoxic microenvironment of tumor tissue to achieve efficient cellular internalization of nanocarriers, on-demand release of the photosensitizer and enhanced site-specific tumor cell killing effect by hypoxia-activated prodrug tirapazamine (TPZ).[8] High cellular uptake can ensure the maximum amount of photosensitizer in the tumor cells, rapid cargo release can overcome the shortcomings of limited diffusion distance and short half-life of reactive oxygen species (ROS), and hypoxic-activated prodrug TPZ can improve the anti-tumor effect of PDT in relatively hypoxic areas.[9,10,12,17]

The employment of hypoxia- and singlet oxygen-responsive polymeric micelles for anti-tumor therapy can address the aforementioned issues. Azobenzene moiety and nitroimidazole (NI) part are two conventional groups for the construction of hypoxic responsive micelles.[18–21] Azobenzene moiety was used to attach hydrophilic groups to hydrophobic parts, and hypoxia-induced reduction of azobenzene could lead to hydrophilic group shedding and enhanced cellular uptake.[17] The NI parts were commonly attached to the hydrophobic part of the amphiphilic copolymer and were converted to hydrophilic amino imidazole under hypoxic conditions, resulting in micelle decomposition.[7,20] Previous work has demonstrated that NI-containing micelles could oxidize by singlet oxygen to get hydrophilic oxamic aldehyde, leading to rapid cargo release.[7] In addition, all the triggers were also expected to show interactive synergism. The hypoxia- and singlet oxygen-responsiveness could not only increase the amount of photosensitizer available for effective PDT therapy, but also improve the degree of hypoxia in tumor tissue, and hence, in turn, enhance the degree of cell uptake and cargo release of nanoparticles.[22–24]

In this study, we developed a kind of "one stone third birds"drug delivery system to improve the photodynamic and chemotherapy anticancer therapeutic efficacy in breast cancer. This drug delivery system, abbreviated as mPEG-Azo-P (Asp-NI)-Ce6 was made up of three main constituents: the hypoxia-induced cleaved azobenzene (Azo) bridges to respond to hypoxia microenvironment for enhanced cellular uptake, the hypoxia- and singlet oxygen-responsive NI group attach to hydrophobic poly (aspartic acid) (P(Asp-NI)) as a hydrophobic segment, which decorated with photosensitizer chlorine e6 (Ce6), and the hydrophilic poly (ethylene glycol) (PEG) was used as a hydrophilic part (Scheme S1 and Scheme S2). The novel hypoxia- and singlet oxygen-responsive polymer could self-assemble to form micelles. The hypoxia-activated chemotherapy prodrug TPZ was selected as the model drug that was physically loaded in the micelles. After the micelles accumulated in the tumor site through enhanced permeability and retention (EPR) effect, Ce6 was induced by laser treatment to produce reactive oxygen species (ROS) for PDT. In addition, PDT-induced consumption of oxygen not only activated TPZ to perform an antitumor effect in the relatively hypoxic area of the tumor site, but also particle internalization enhancement as well as triggered on-demand photosensitizer release, resulting in a synergistic photodynamic and chemotherapy therapeutic effect (Scheme 1).

Materials and Methods

Materials

N-(3-bromopropyl) phthalimide, ethyl acetate, 4.4-azodiphenylamine, cyclohexane, carbodiimide (EDC), dichloromethane, tetrahydrofuran, sodium hydride, *N, N*-diisopropyl diimide, ice ethyl ether, formamide, Chlorin e6 (Ce6), tirapazamine (TPZ), triethylamine (TEA), 1, 3-diphenylisobenzofuran (DPBF), sodium hydrosulfite ($Na_2S_2O_4$), dimethyl sulfoxide (DMSO) were purchased from McLean Biochemical Technology Co., Ltd. (Shanghai, China). mPEG-NHS was purchased from Shanghai Proglo Biotechnology Co., LTD. Methanol, acetonitrile, and absolute ethanol (C_2H_5OH) were supplied by Sinopharm holding Shanghai Chemical Reagent Co., Ltd. Hydrochloric acid and chloroform were purchased from Tianjin Jiangtian Chemical Technology Co., LTD. *L*-aspartate *β*-benzyl ester, *N, N*-dimethylformamide (DMF), 2-nitroimidazole, and *N*-bromosuccinimide were purchased from Tianjin Siensi Biochemical Technology Co., LTD. Hydrazine was purchased from Beijing Coupling Technology Co., LTD. Sodium carbonate and sodium sulfate were purchased from Shanghai Aladdin Co., LTD. DMEM medium was purchased from Gibco (USA). Fetal bovine serum (FBS) was purchased from Zhejiang Tianhang Biotechnology Co., LTD. Methyl thiazole diphenyl tetrazolium bromide

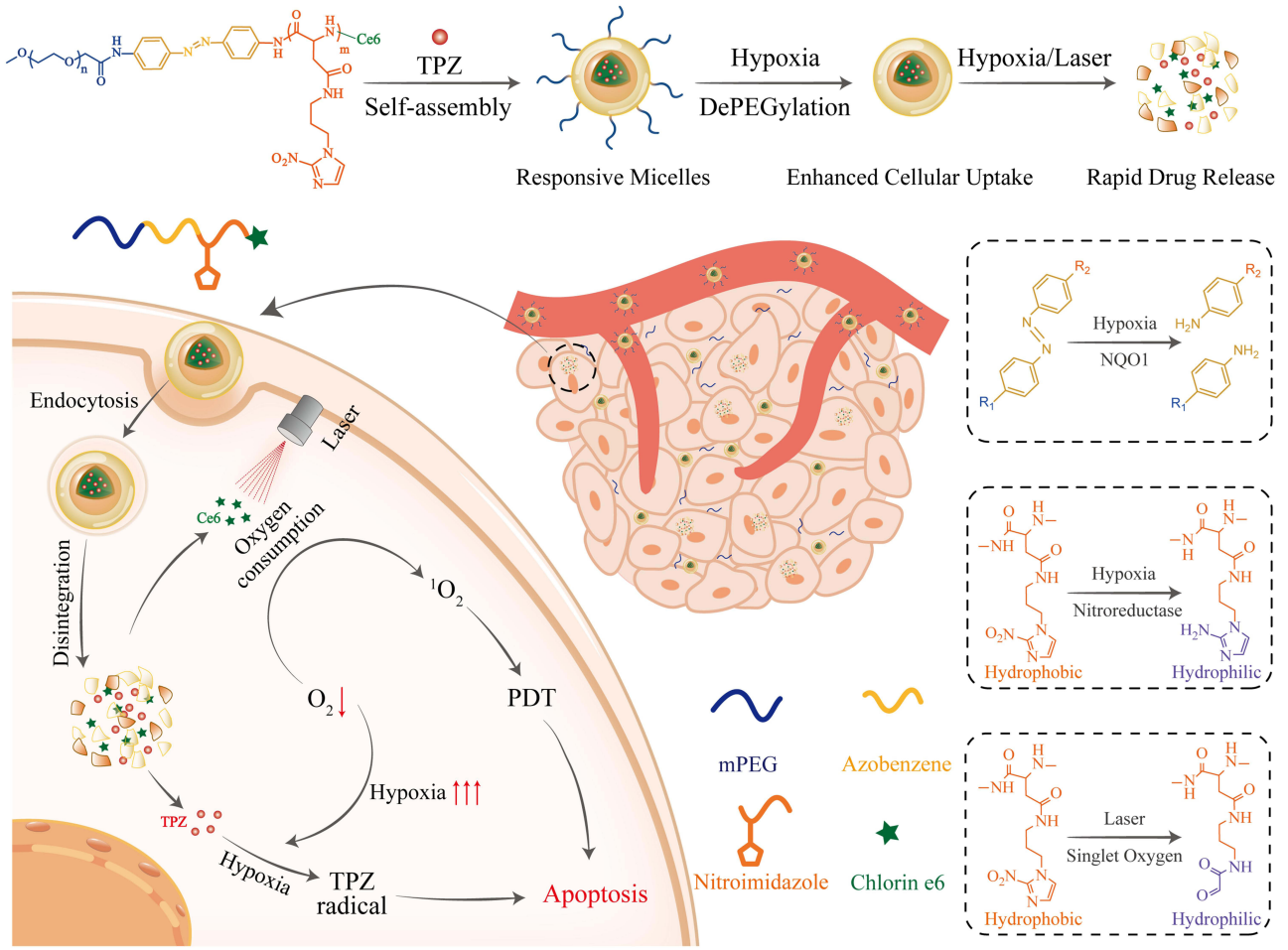

Scheme 1 Hypoxia- and singlet oxygen-responsive polymeric micelles for in tegration of photodynamic and chemotherapy therapy in a tumor-bearing mice model.

(MTT) was purchased from Biofroxx (Einhausen, Germany). Calcein/PI cell viability and cytotoxicity test kit, trypsin cell digest, and reactive oxygen species test kit were purchased from Shanghai Biyuntian Biotechnology Co., Ltd.

Animals and Cell Culture

BALB/c mice were purchased from Henan Sikebeisi Biotechnology Co., LTD. The animal experimental procedure was approved by The Animal Health Committee of Bengbu Medical College (Licence No. 2023168), which met the requirements of the Animal Ethical Standards and Use Committee of Bengbu Medical College. Mouse breast carcinoma 4T1 cells were purchased from Kunming Cell Bank, Chinese Academy of Sciences. The cells were cultured in DMEM high glucose medium containing 10% fetal bovine serum (Gibco Co., Ltd) and 1% penicillin. Under normoxic conditions, the cells were kept at 37°C in a humidified atmosphere containing 5% CO_2. Under hypoxic conditions, the cells were incubated in a modular incubator chamber (Billups-Rothenberg) that was supplemented with a humidified gas mixture (1% O_2, 5% CO_2, and 94% N_2). When the cell confluence reached 80–90%, the cells were digested with 0.25% trypsin-EDTA and used for subsequent experiments.

Synthesis of mPEG-Azo-P (Asp-NI)-Ce6

The amphiphilic polymer mPEG-Azo-P (Asp-NI) (DHM) was synthesized according to our recently published method.[17] The Ce6-conjugated mPEG-Azo-P (Asp-NI)-Ce6 (DHM-Ce6) was obtained via amidation reaction. Firstly, Ce6 (69.7 mg, 0.10 mmol), EDC (230.04 mg, 1.2 mmol), and NHS (46.03 mg, 0.4 mmol) were dissolved in 20 mL formamide. The mixture solution was protected by nitrogen and stirred at room temperature for 3 h. Then, the DHM

(200 mg, 0.02 mmol) solution in anhydrous formamide (10 mL) was added. The mixture was kept at 25°C for 24 h under nitrogen protection. After 2 days of dialysis against deionized water (MWCO, 3500 Da), free Ce6 was removed by filtration with 0.45 μm membrane, followed by freeze-drying to get DHM-Ce6 (yield: 71%).

Micelle Preparation and Characterization

The preparation of amphiphilic conjugated micelles was prepared by film hydration method.[12] In brief, 30 mg DHM-Ce6 and 3 mg Tirapazamine (TPZ) were dissolved in 25 mL acetonitrile and ultrasonic-assisted dissolution was performed. After the removal of the solvent by rotary evaporation, 30 mL of deionized water was used for hydration at room temperature and the mixture was stirred for 45 min. After centrifugation (2000 rpm, 5 min), followed by 2 days of dialysis against deionized water (MWCO, 3500 Da), the deionized water was refreshed every 6 h, the hydrated solution was filtered by 0.45 μm filtration membrane to remove excess TPZ. Then the solution was freeze lyophilized to get DHM-Ce6@TPZ. The particle size and Zeta potential of DHM-Ce6 and DHM-Ce6@TPZ were determined by Zetasizer Nano ZS (Nano-ZS290). The morphology of the above micelles was observed by transmission electron microscopy (TEM, Hitachi, Regulus-8100). Ultraviolet-vis (UV-vis) spectra of DHM-Ce6@TPZ micelles in deionized water were recorded with ultraviolet spectrophotometer (UV-2700), free Ce6, free TPZ, DHM, and DHM-Ce6 were used as the controls. The amount of TPZ and Ce6 was measured by the UV-vis spectrum at 467 nm of TPZ and 404 nm of Ce6. All the measurements were performed three times, and the mean plus SD was used to present the data.

Stimuli-Responsiveness Assessment

The DHM-Ce6 micelles (0.5 mg/mL) were mixed with sodium dithionite with a concentration of 10 mM. After incubation at ambient temperature for a designated time, the UV-vis absorption spectra of the mixture were recorded. The effect of singlet oxygen treatment on DHM-Ce6@TPZ micelles was investigated using TEM size as the major indicator. The DHM-Ce6@TPZ micelles (0.5 mg/mL) in PBS buffer were irradiated (660 nm, 200 mW/cm^2, 10 min) at ambient temperature (25°C) according to previous literature.[12] The irradiation-free samples were used as the control. The drug release kinetics from DHM-Ce6@TPZ micelles under hypoxic conditions was performed using the static Franz cell method, which consists of a donor chamber and receptor chamber. In brief, the regenerated cellulose membrane with a molecular weight cut-off (MWCO) of 1000 Da was used to separate the two chambers. The donor chamber contained 2 mL of DHM-Ce6@TPZ aqueous solution (2.5 mg/mL). The receiving fluid was sodium dodecyl sulfate (5%, w/w) aqueous solution with or without sodium dithionite (10 mM) and stirred by a magnetic bar. Sodium dithionite was used to mimic the hypoxic condition. Finally, the collected samples at designated time points were subjected to UV analysis for determining the extent of TPZ release. The drug release kinetics from DHM-Ce6@TPZ micelles under laser irradiation was performed with a similar method with the laser treatment to the sample lasted for 10 min (660 nm, 200 mW/cm^2). The micelles without laser treatment were used as the negative control.

In vitro Singlet Oxygen Production

The ability of the micelles to produce ROS was studied by 1.3-Diphenylisobenzofuran (DPBF) probe. The structure of DPBF can be destroyed by ROS that leads the fluorescence quenching, and the ability of the micelles to produce ROS could be indirectly measured by measuring the fluorescence quenching of DPBF. In brief, 5 μM DPBF which dissolved in DMSO was mixed with PBS, free Ce6 (10 mM), DHM-Ce6, and DHM-Ce6@TPZ solution, respectively. The dose of Ce6 was fixed at 10 mM of DHM-Ce6 and DHM-Ce6@TPZ solutions. All samples were irradiated with 660 nm near-infrared light (200 mw/cm^2, 5 min). Compared with an exposure time of 10 minutes used in stimuli-responsive experiments, 5 minutes was chosen for singlet oxygen production, which could ensure the survival rate of cells while detecting enough ROS. Then, based on the absorption intensity at 411 nm, the absorption spectrum of the mixture was determined at the fixed time with an ultraviolet-visible spectrophotometer.

Cellular Uptake

The cellular uptake of DHM-Ce6@TPZ in 4T1 cells was observed by confocal laser scanning microscopy (CLSM). 4T1 cells were seeded in a 20 mm glass bottom cell culture dish (2×10^4 cells per well) and cultured in DMEM medium at

37°C for 24 h, then the samples were continued to be cultured under hypoxic conditions for 12 h. Then the cells were incubated with DHM-Ce6@TPZ under hypoxia. After a predefined time (2 h, 4 h, and 6 h), the cells were washed with PBS and immobilized with 4% paraformaldehyde for 10 min. Finally, the cell nuclei were labeled with DAPI (1 μg/mL in PBS) for 5 min and observed with CLSM. The excitation wavelengths Ce6 was 488 nm, and the emission wavelengths were 525 nm respectively. Similarly, the cellular uptake of micelles under normoxic conditions was performed as a similar method without the use of the hypoxia chamber.

Cell Viability

The cytotoxicity of micelles was analyzed by the standard MTT method. 4T1 cells were seeded in 96-well plates with 5×10^3 cells per well. After 24 h standard incubation at 37°C, the cells were further incubated for 12 h under normoxia or hypoxia. Then, the cells were incubated with DHM-Ce6 or DHM-Ce6@TPZ for 4 h under normoxic or hypoxic conditions. The concentrations of TPZ ranged from 0 to 5 μg/mL, and the dose of DHM-Ce6 and DHM-Ce6@TPZ were set to match that of TPZ concentrations. Laser irradiation was applied using the 660 nm laser at the power of 200 mW/cm^2 for 5 min if needed, laser-free samples were used as controls. Then all treatment groups were incubated for another 12 hours. After removing the original medium, 100 μL of fresh medium containing 50 μg MTT per well was added to each well and incubated at 37°C for 4 h. Then, the supernatant in each well was removed, 100 μL of DMSO was added and the plates were shaken for 20 min at a suitable temperature. The viability of 4T1 cells in response to DHM with or without laser irradiation under normoxia was determined by the same method. The half maximal inhibitory concentration (IC_{50}) of the three formulations under different conditions was calculated. The cytotoxicity of the three formulations was also assessed by the standard protocol of fluorescence staining of live/dead cells with calcein-AM (4 μM, Ex/Em = 488 nm/520 nm) and PI (2 μM, Ex/Em = 561 nm/620 nm) probes. The experiments were carried out under hypoxia or normoxia with or without laser treatment. To determine the cytotoxicity of DHM-Ce6 and DHM-Ce6@TPZ micelles to normal cells, the 3T3 mouse embryonic fibroblast cells were used in this section. Briefly, 3T3 cells were inoculated in a 96-well plate with 5×10^3 cells per well. After 24 h standard incubation at 37°C, the cells were further incubated for 12 h under normoxic conditions. The cell viability was measured by colorimetric MTT assay. Other details were confirmed according to aforementioned experiments.

Apoptosis Assay

The Annexin V-FITC/PI double staining apoptosis assay kit was used to quantitatively determine the number of apoptotic cells. 4T1 cells were seeded in six-well plates at 3×10^5 cells per well overnight under normoxia or hypoxia, the cells were exposed to two formulations, including DHM-Ce6 and DHM-Ce6@TPZ (n = 3). Four hours later, the cells were irradiated by the 660 nm laser for 5 min. The cells without laser treatment were used as the controls. After another 12 h's incubation, all cells were collected and resuspended in the Annexin V binding solution. The cells were stained with Annexin V-FITC and PI, followed detected by flow cytometry immediately.

Intracellular ROS Detection

In vitro ROS generation in 4T1 cells was detected using 2′,7′-dichlorodihydrofluorescein diacetate (DCFH-DA). 4T1 cells were seeded in a 20 mm glass bottom cell culture dish at a density of 2×10^4 cells per well. After 24 h standard incubation at 37°C, the cells were further incubated for 12 h under normoxic conditions or hypoxic conditions. Then, the samples of PBS, TPZ, DHM-Ce6, and DHM-Ce6@TPZ were added to the plates and incubated with the cells for 4 h under hypoxia or normoxia, followed by PBS washing in triplicate. Then fresh medium containing the DCFH-DA probe (10 μM) was added and incubated for another 30 min at 37°C. Laser irradiation was applied using a 660 nm laser at a power of 200 mW/cm^2 for 5 min if needed, laser-free samples were used as controls. Finally, the fluorescence imaging was recorded (Ex: 488 nm, Em: 525 nm).

Ex vivo Biodistribution

This study was conducted in strict accordance with recommendations with the guidelines set by the local regulatory body and was approved by the Institutional Animal Care and Use Committee of Bengbu Medical College (Bengbu, China). To

track the biodistribution of the micelles after intravenous injection, a fluorescent probe Cy5 was physically encapsulated in DHM to obtain DHM-Cy5. Female BALB/c mice of 4–6 weeks of age were purchased from Henan Sikebeisi Biotechnology Co., LTD. 1×10^6 4T1 cells in 0.05 mL of PBS were implanted into the BALB/c mice. When the average tumor volume reached about 200 mm^3, 150 μL formulations (free Cy5, DHM-Cy5 micelles) were intravenously injected into the mice through the tail vein with a fixed Cy5 dose at 2 mg/kg (n = 3). At different time points post-administration (2, 4, 6, 8, and 24 h), the mice were scanned via a Cri Maestro in vivo imaging instrument. The Cy5 excitation wavelength was 630 nm and the emission wavelength was 700 nm. The average fluorescence intensity of Cy5 in the tumor was plotted against time. After 48 h, the animals were sacrificed, and the tumors and major healthy organs (heart, liver, spleen, lung, kidney) were obtained for fluorescence imaging.

In vivo Antitumor Study

When the tumor volume reached about 100 mm^3, the 4T1 xenograft-tumor-bearing BABL/c mice were randomly divided into 6 groups (5 mice per group): (1) PBS with laser irradiation, (2) Free TPZ with laser irradiation, (3) DHM-Ce6 without laser irradiation, (4) DHM-Ce6 with laser irradiation, (5) DHM-Ce6@TPZ without laser irradiation, (6) DHM-Ce6@TPZ with laser irradiation. All samples were administrated via the tail vein, respectively. The dose of Ce6 was 5 mg/kg. After 8 h, the mice were irradiated by a laser (660 nm, 200 mW/cm^2) for 30 min if needed. The tumor volume and body weight of mice were measured every two days. The volume of the tumor was calculated as follows:

$$V = \frac{a \times b^2}{2}$$

V is the tumor volume, a is the tumor length, and b is the tumor width.

In the equation, a represents the maximum diameter of the tumor and b represents the minimum diameter of the tumor. At the end of the experiment, the tumor tissues were collected for histological (H&E) staining and apoptotic (TUNEL) staining according to commercial assay kits and published protocols, respectively. At the end of the efficacy study, H&E staining was also performed on major healthy organs to analyze the biocompatibility and adverse effect determination.

Statistical Analysis

The data were presented as mean ± standard deviation. Significant difference was compared via either Student's *t*-test or analysis of variance coupled with Tukey's post hoc analysis. Differences in data were considered statistically significant at $P < 0.05$.

Results and Discussion

Synthesis of mPEG-Azo-P (Asp-NI)-Ce6

To validate our design, we selected azobenzene fragments as hypoxic response junctions, covalently linking hydrophilic mPEG and hydrophobic nitroimidazole fragments together. The synthetic method of amphiphilic polymer containing both azobenzene and nitroimidazole groups contained four major steps (Scheme S1 and Scheme S2). Firstly, the azobenzene group was connected to the mPEG terminal to obtain amine-bearing mPEG (mPEG-Azo-NH_2). Then, mPEG-Azo-NH_2 was used as the initiator to induce the polymerization of aspartic acid *N*-carboxy anhydride. The hypoxia-responsive intermediate mPEG-Azo-P (Asp-NI) was obtained through a polymerization method, and the nitroimidazole group was connected to the polypeptide backbone.[17] Finally, Ce6 molecules were conjugated to the polymer chain by amidation reaction to provide hypoxia and singlet oxygen dual-responsive polymer mPEG-Azo-P (Asp-NI)-Ce6.

The intermediate and target polymer was purified by appropriate methods, and the structures were confirmed by nuclear magnetic resonance spectroscopy (^{1}H NMR) (Figure S1). On the basis of the proton nuclear magnetic resonance spectra, the average molecular weight (MW) of the designed polymer was approximately 9960 Da (DHM) and 10,560 Da (DHM-Ce6) respectively. The molecular weight difference between the two polymers is roughly equal to the mass of

Ce6. The degree of amino acid polymerization was about 18. The average conjugation degree of the polymer to nitroimidazole reached about 100%, which was due to the high ammonolysis efficiency of excess nitroimidazole.

Preparation and Characterization of mPEG-Azo-P (Asp-NI)-Ce6 Micelles

The responsive polymer MPEG-Azo-P (Asp-NI)-Ce6 micelles (DHM-Ce6) were prepared by a representative membrane hydration method. The TPZ-loaded micelles (DHM-Ce6@TPZ) were also provided with the same method. The presence of TPZ increased the dynamic light scattering size of DHM-Ce6 micelles from 171 ± 12 nm to 189 ± 15 nm (DHM-Ce6 @TPZ) (Figure 1A). The increase in particle size is a typical phenomenon of drug loading in micelles, which was the result of the expansion of the micellar core induced by drug loading.

Through transmission electron microscopy (TEM), we found that DHM-Ce6 and DHM-Ce6@TPZ maintained the spherical structure with an average size of about 150 nm and 170 nm, which was smaller than the average hydrodynamic diameter in aqueous solution measured by dynamic light scattering (DLS) (Figure 1A–1C). The TPZ loading of DHM-Ce6 @TPZ was about 7.38% (w/w) (Figure S2). The homogeneous morphology of DHM-Ce6 and DHM-Ce6@TPZ were also demonstrated by scanning electron microscope (SEM), which were coincident well with TEM results (Figure S3). Based on

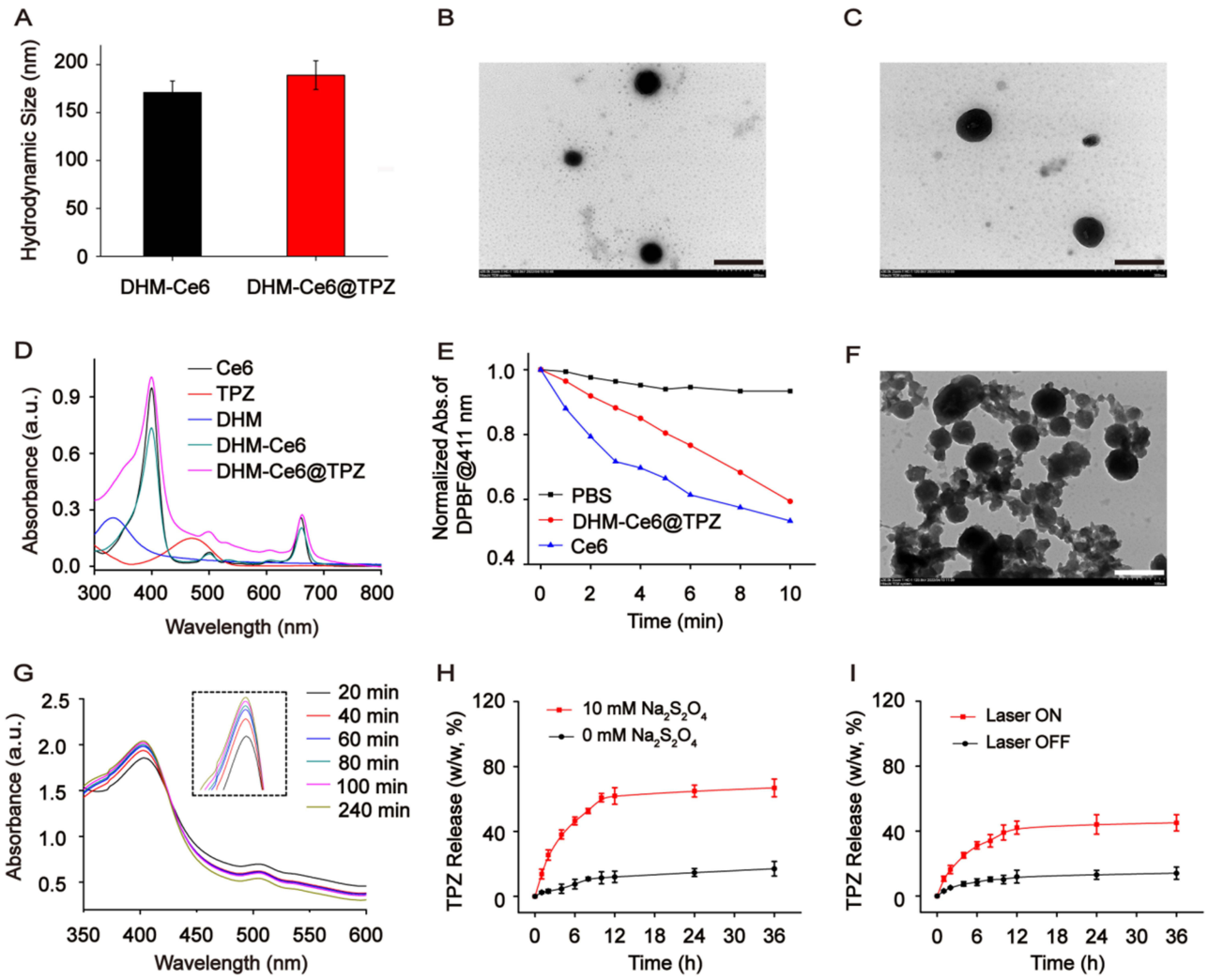

Figure 1 Physicochemical properties of hypoxia and singlet oxygen-responsive micelles (n = 3). (**A**) The hydrodynamic size of DHM-Ce6 and DHM-Ce6@TPZ. Transmission electron microscope images of DHM-Ce6 (**B**) and DHM-Ce6@TPZ (**C**) (scale bar: 500 nm). (**D**) UV-vis absorption spectra of Ce6, TPZ, DHM, DHM-Ce6, and DHM-Ce6@TPZ. (**E**) Normalized absorbance of DPBF at 411 nm of different formulations with light irradiation. (**F**) TEM image of DHM-Ce6@TPZ micelles post laser treatment (660 nm, 200 mW/cm^2, 10 min). Scale: 500 nm. (**G**) The UV-vis spectra of DHM-Ce6@TPZ treated with sodium dithionite (10 mM). TPZ release from DHM-Ce6@TPZ micelles under mimicked hypoxia conditions. (**H**) (10 mM sodium dithionite), and under laser irradiation conditions (**I**) (660 nm, 200 mW/cm^2, 10 min).

the UV-vis absorption intensity at 650 nm, approximately 4.2 wt % of Ce6 was conjugated to the chain (Figure S2). As shown in Figure 1D, the UV-vis spectra showed a remarkable absorption peak at 330 nm which was attributed to azobenzene groups, and the absorption peaks of DHM-Ce6@TPZ at 463 and 670 nm revealed that TPZ (463 nm) and Ce6 (670 nm) were successfully loaded into the micelle.[9] The ROS generation capacity of DHM-Ce6@TPZ was evaluated under near-infrared irradiation. As a typical ROS indicator, the absorption of 1.3-diphenylisobenzofuran (DPBF) at 407 nm could be quenched by ROS sensitively. As shown in Figure 1E, the absorption of DPBF at 407 nm rapidly decayed within 10 min after light irradiation, confirming that DHM-Ce6@TPZ could produce large amounts of ROS that can be used in photodynamic therapy. After laser treatment, the spherical structure of DHM-Ce6@TPZ micelle was destroyed. This was attributed to the singlet oxygen produced by Ce6 oxidizing the NI moiety to aldehyde, resulting in micelle degradation (Figure 1F).[7] The intracellular reduction of the nitroimidazole group under hypoxic conditions requires the catalysis of nitroreductase with the presence of nicotinamide adenine dinucleotide phosphate (NADPH) that donates electrons and aids as the reducing agent.[17,25] To mimic such a reaction in vitro, a reducing agent, sodium dithionite sodium dithionite ($Na_2S_2O_4$), was mixed with DHM-Ce6@TPZ micelles to simulate the drug release under hypoxic conditions. The release experiments under normoxic conditions were presented with the concentration of $Na_2S_2O_4$ at 0 mM. The supplement of a single nitroreductase plus NADPH in buffers could not mimic the intracellular conditions, so an inorganic reducing agent sodium dithionite was used for proof-of-concept in vitro.[17,25–28] The presence of sodium dithionite significantly sped up the cargo release, this was because sodium dithionite donates electrons to azobenzene and nitroimidazole groups, leading to polymer degradation and micelle disintegration (Figure 1G and H). As shown in Figure 1I, the release rate and degree of TPZ after laser treatment is significantly higher than that without laser irradiation, this phenomenon was attributed to the imidazole moiety could oxidize to hydrophilic oxamic aldehyde, resulting in micelle disassembly. Such a distinction would promote the rapid cargo release upon triggering, which was ideal to solve the problem of limited diffusion radius and short lifetime of singlet oxygen in PDT.[7] Therefore, all of the results demonstrated that the structure of DHM-Ce6@TPZ can be disintegrated when triggered with hypoxia and singlet oxygen, along with a rapid release of TPZ.

Enhanced Micelles Uptake Under Hypoxia

To examine the cellular uptake of DHM-Ce6@TPZ, murine breast cancer cell line 4T1 cells were incubated with DHM-Ce6@TPZ at 37°C for 4 h and then observed by confocal laser scanning microscope (CLSM). Under hypoxic conditions, the fluorescence intensity of Ce6 in DHM-Ce6@TPZ was significantly higher than under normoxic conditions at all three investigated time points (Figure 2 and Figure S4). This phenomenon can be explained by the hypoxia-induced

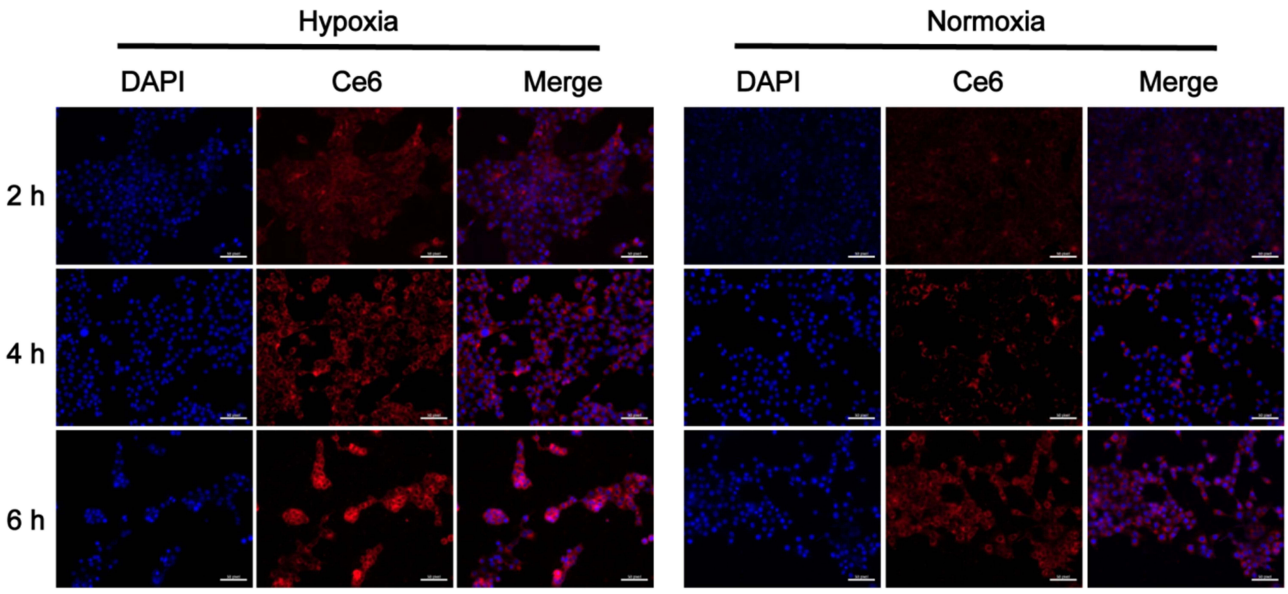

Figure 2 Confocal images of cellular uptake by 4T1 cells under normoxia or hypoxia at 2, 4, and 6 h post DHM-Ce6@TPZ micelles incubation (scale bar: 20 μm, n = 3).

azobenzene reduction and subsequent PEG shedding. Azobenzene reductase would be overexpressed in the hypoxic microenvironment, which could destroy the azobenzene bond resulting in micelles disintegration. Our previous work has demonstrated the azobenzene-containing micelles displayed an enhanced cellular uptake compared to the azobenzene-free micelles.[17]

Cell Viability

3-(4, 5-dimethylthiazol-2-yl)-2,5-diphenyltetrazolium bromide (MTT) assay was used to evaluate the cytotoxicity of DHM-Ce6@TPZ against 4T1 cells. High cell viability of the resulting polymeric micelles without Ce6 (eg, DHM) was observed at high concentrations independent of light and oxygen, demonstrating the safety of the DHM micelles (Figure S5). Under normoxic conditions and no laser irradiation, the cells treated with DHM-Ce6, and DHM-Ce6@TPZ proved no decent cytotoxicity because the highly reactive singlet oxygen was not generated (Figure 3A and Figure S6). In sharp contrast, after 5 min of light irradiation (660 nm, 200 mW/cm^2) the viability of 4T1 cells treated with DHM-Ce6, and DHM-Ce6@TPZ evidently reduced (Figure 3B and C, Table S1). The IC_{50} value of the samples in the normoxic under laser irradiation conditions was in the order of DHM-Ce6@TPZ<DHM-Ce6 (IC_{50}/Ce6: 0.363 ± 0.042/μg mL and 0.412 ± 0.056 μg/mL, respectively, Figure S7). When added a stimulus of the hypoxic microenvironment to 4T1 cells, DHM-Ce6@TPZ showed significant cytotoxicity in a hypoxic environment without light irradiation, and DHM-Ce6 groups still maintained as almost invariant (Figure 3A and Figure S6). This phenomenon was attributed to no singlet oxygen should be produced as no laser was applied, and the cytotoxicity was presumed due to the contribution of TPZ.[29] After exposure to light irradiation the viability of the 4T1 cell incubated with DHM-Ce6@TPZ was lowest among all groups and much lower than itself without light irradiation (Figure 3A). Interestingly, the IC_{50} value of the DHM-Ce6@TPZ and DHM-Ce6 in the hypoxic microenvironment under light treatment showed a huge difference (IC_{50}/Ce6: 0.211 ± 0.019 μg/mL and 0.875 ± 0.05 μg/mL, respectively) (Figure 3B and C,

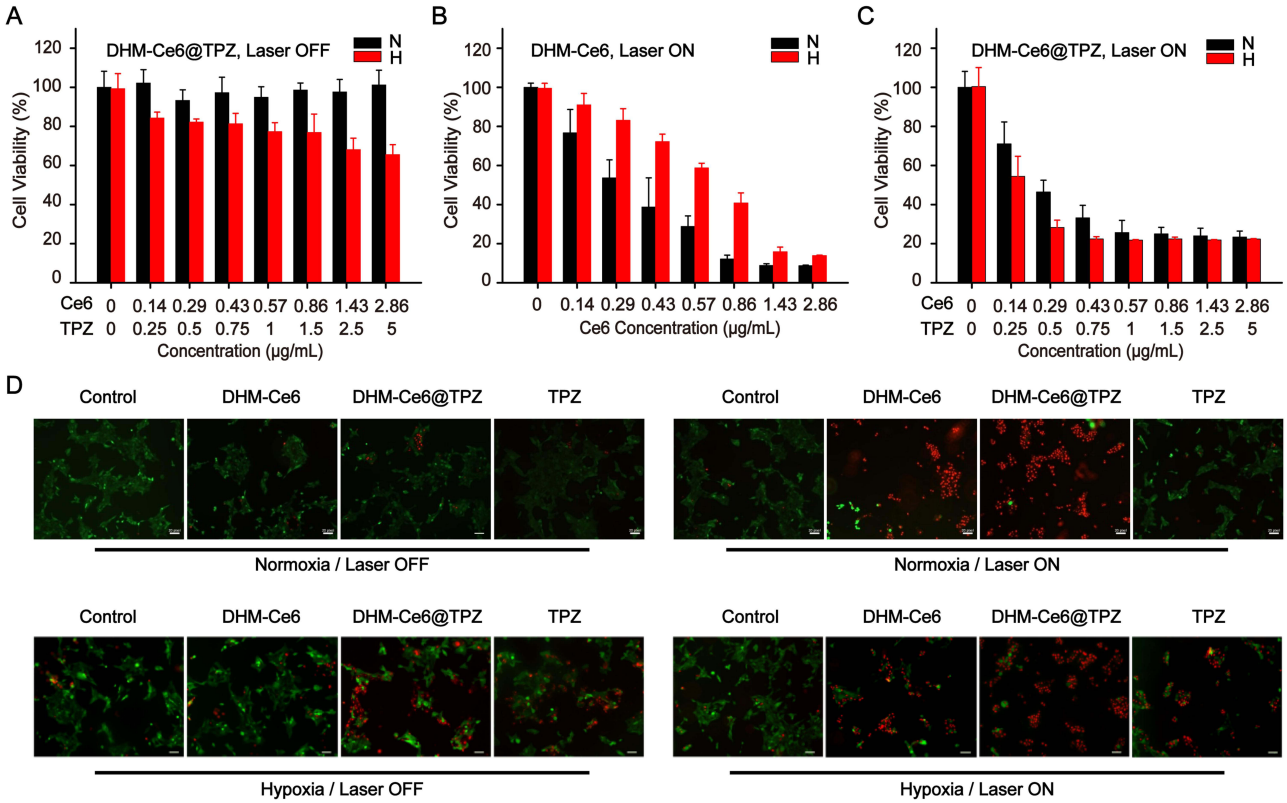

Figure 3 Viability of 4T1 cells in response to different formulations treatment under normoxia or hypoxia.(n = 4) (**A**) DHM-Ce6@TPZ without laser irradiation under normoxia or hypoxia. (**B**) DHM-Ce6 with laser irradiation under normoxia or hypoxia. (**C**) DHM-Ce6@TPZ without laser irradiation under normoxia or hypoxia. (**D**) Imaging of living and dead cells upon formulation treatment with the fixed TPZ dose at 1 μg/mL. The cells were stained with Calcein AM (green, live cells) and PI (red, dead cells) (scale bar: 20 μm).

Table S1). Such an obvious cytotoxicity difference was assumed due to hypoxia-induced azobenzene reduction and subsequent PEG shedding, Ce6-mediated PDT aggravated hypoxia-induced micelle degradation and enhanced cargo release and hypoxia-activated cytotoxicity of TPZ.[7,8,17]

The vivid live-dead cell staining analysis of different formulations under normoxic and hypoxic conditions coincided well with the cell viability results (Figure 3D). Because of the irradiation alone may damage the tumor cells, the control groups of Figure 3D was used as the controls. The intracellular ROS was used as another index to assess the anti-tumor potency of the dual hypoxia- and singlet oxygen-responsive micelles. The TPZ-loaded micelles showed a higher ROS under hypoxia compared to that under normoxic conditions. Consistent well with the cell viability assay, the DHM-Ce6 @TPZ was more powerful in inducing ROS than DHM-Ce6 at the same TPZ dose under hypoxic conditions (Figure 4 and Figure S8), which was contributed by the hypoxia-induced azobenzene reduction and enhanced cellular uptake, singlet oxygen-induced NI oxidation to hydrophilic oxamic aldehyde and rapid cargo release. The discrepancy between the fluorescence intensity under hypoxic conditions and that under normoxic conditions was assumed due to the difference in oxygen concentration. The 3T3 mouse embryonic fibroblast cells were selected as a model of normal cells. As expected, DHM-Ce6 and DHM-Ce6@TPZ micelles displayed no noticeable toxicity to the 3T3 cells without laser irradiation under normoxic conditions (Figure S9). The analysis of apoptosis by flow cytometry was also consistent with the MTT toxicity of DHM-Ce6 and DHM-Ce6@TPZ to 4T1 cells under different conditions (Figure S10).

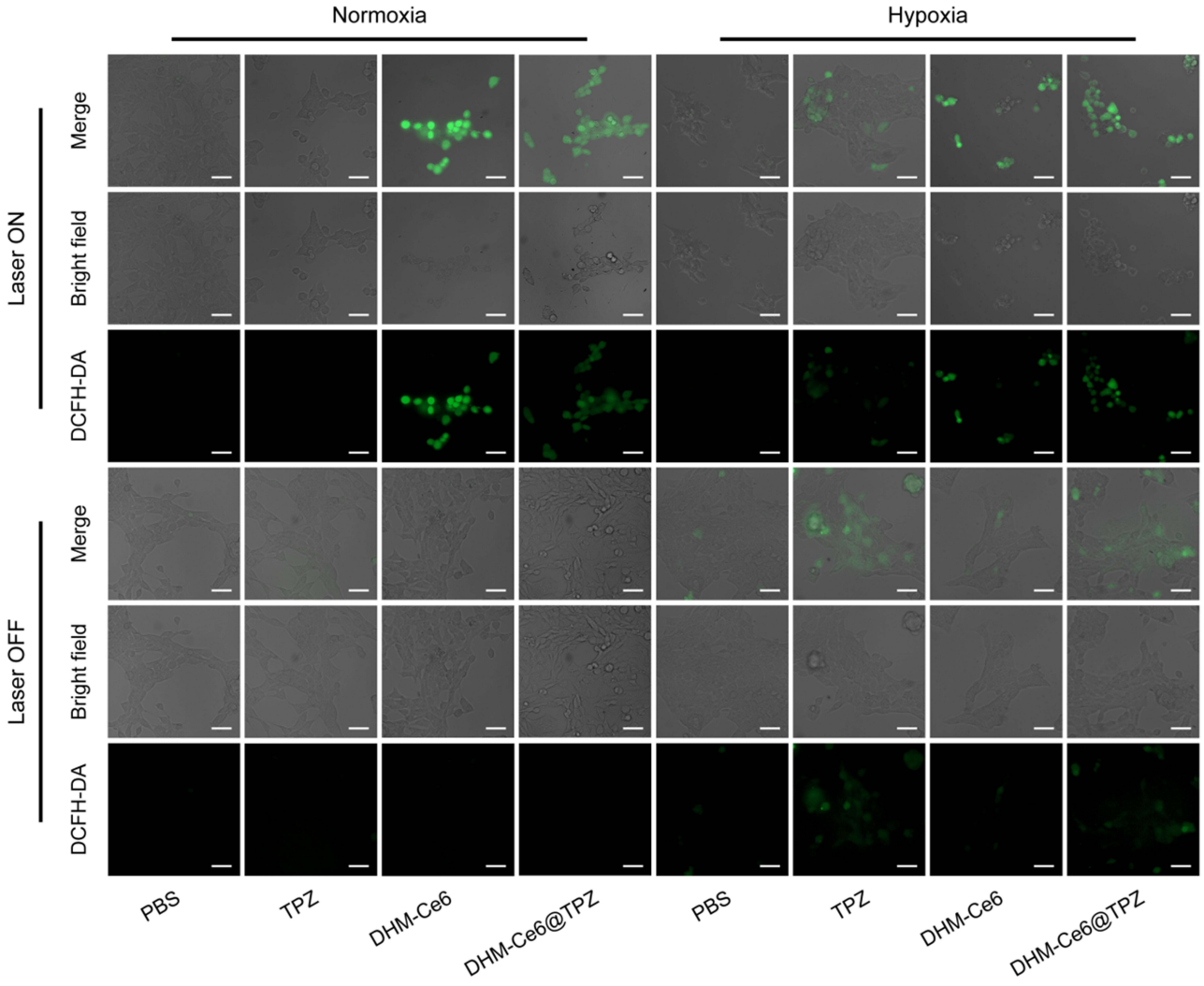

Figure 4 Fluorescence imaging of total reactive oxygen species (ROS) in 4T1 cells upon formulation treatment under different conditions, ROS was performed using a DCFH-DA probe (scale bar: 50 μm) with the dose of TPZ fixed at 1 μg/mL (n = 3).

Biodistribution

Although both TPZ and Ce6 show intrinsic fluorescence, a fluorescent probe (Cy5) was used to label the micelles (DHM-Cy5) to study the in vivo biological distribution of micelles, and free Cy5 was used as the control. This was because the fluorescence probe Cy5 has a long excitation and emission wavelength, making it an ideal candidate for micelles location imaging agent in mice.[30] As shown in Figure 5A, both the formulation and free Cy5 exhibited kinetic tumor deposition curves. In contrast to the control formulation, the micelles could deliver more cargo to the tumor site at all five time points (2 h, 4 h, 6 h, 8 h, and 24 h), which was mainly a consequence of the enhanced permeability and retention (EPR) effect.[31,32] Compared to the control, the content of the Cy5 probe in the tumor was much higher for DHM-Cy5 micelles ($p < 0.001$) (Figure 5B and C). The kinetic tumor deposition curves of DHM-Cy5 micelles reached the peak at 8 h after injection, which was consistent with previous investigations (Figure 5B).[33] After 24 h post injection, the mouse was killed and the main organs and tumor were obtained for ex vivo fluorescence imaging. As shown in Figure 5C and D, the micelles were mainly accumulated in the liver, spleen, and tumor. These results suggested that DHM-Cy5 micelles could be effectively accumulated at the tumor site after intravenous injection. Both free Cy5 and DHM-Cy5 micelles also existed in other major healthy organs (heart, liver, spleen, lung, and kidney) because of the non-specific biodistribution.

In vivo Antitumor Efficacy

The therapeutic effects of the dual hypoxia- and singlet oxygen-responsive micelles were verified by subcutaneous implantation of 4T1 cells to establish a xenograft mouse model. As shown in Figure 6A, the tumor volume of the mice in the DHM-Ce6 without laser treatment group reached 1435 ± 298 mm^3 after 21 days of treatment, which was similar to the tumor size of the TPZ with laser irradiation (1386 ± 416 mm^3). The group of free Ce6 under laser irradiation was used as control to investigate the therapeutic effects of the dual hypoxia- and singlet oxygen-

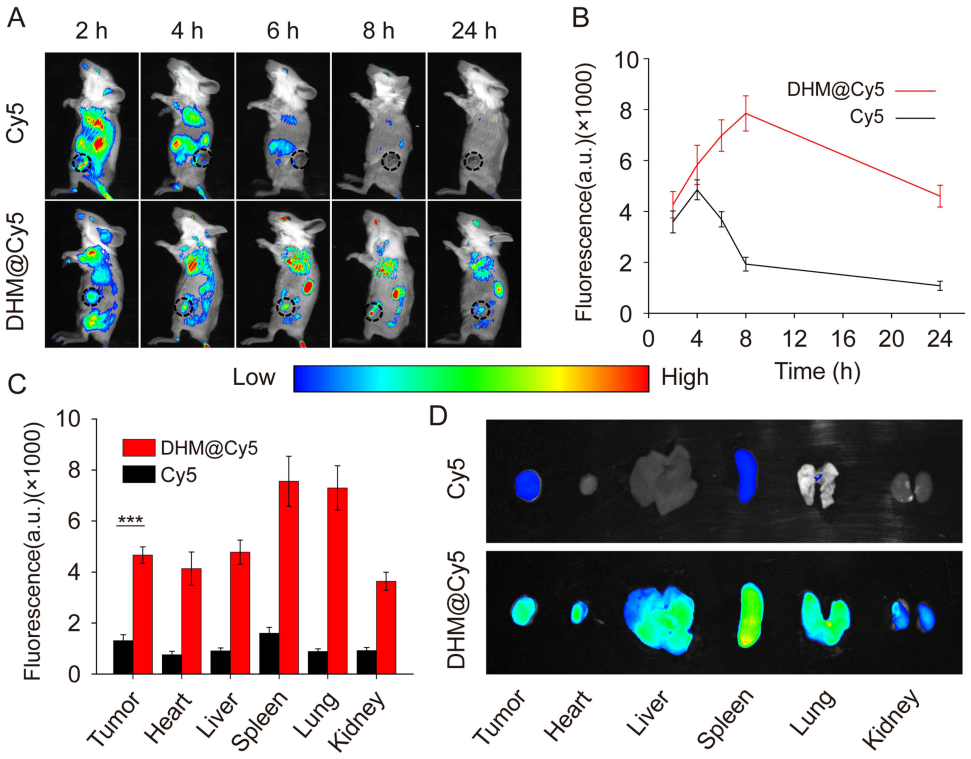

Figure 5 Kinetic biodistribution of micellar formulations in 4T1 tumor-bearing mice (n = 3). (**A**) In vivo kinetic fluorescence of Cy5 in 4T1 tumor-bearing mice up to 24 h after intravenous injection of free Cy5, DHM@Cy5 micelles. (**B**) Kinetic fluorescence quantification regarding Cy5 in tumors. (**C**) Semi-quantitative fluorescence summary of Cy5 level in healthy organs and tumors at the end of the biodistribution study. ***$p < 0.001$. (**D**) Ex vivo fluorescent analysis of Cy5 in tumors and other healthy organs 24 h post-dose administration.

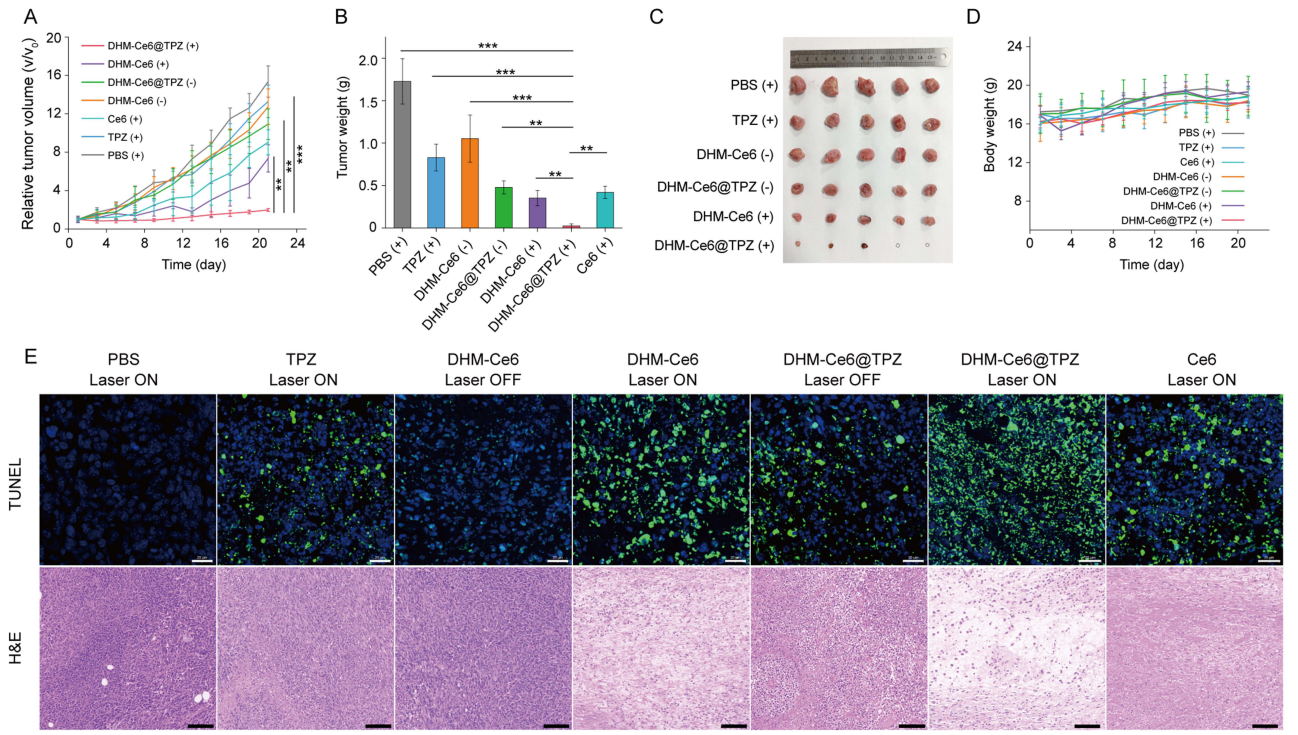

Figure 6 In vivo antitumor efficacy of dual-responsive micelles (n = 5). (**A**) Tumor-growth inhibitory effects of seven formulations. (**B**) Quantitative analysis of tumor weight. (**C**) Images of tumors in the end of treatment. (**D**) Changes in body weight of mice during treatments. (**E**) TUNEL staining (scale bar: 50 μm) and H&E staining (scale bar: 100 μm) at the end of therapy. $^{**}p < 0.01$; $^{***}p < 0.001$.

responsive micelles. Compared with the laser irradiation alone group (eg, PBS under laser treatment group), tumor size was significantly inhibited in the DHM-Ce6@TPZ and DHM-Ce6 treatment groups with inhibition rates of 93.19% and 57.11%, respectively. This large difference in therapeutic effects was thought to be due to hypoxia-induced azobenzene reduction and subsequent enhanced cellular uptake, singlet oxygen-induced NI oxidation, and enhanced TPZ release and hypoxia-activated TPZ cytotoxicity. TPZ-induced chemotherapy is a complement to the effect of PDT, through which the synergistic effect can be achieved. DHM-Ce6@TPZ without laser treatment showed a compromised antitumor effect compared with that under laser treatment (1197 ± 393 mm^3 vs 111 ± 87 mm^3). This phenomenon was attributed to Ce6 could only produce singlet oxygen under laser irradiation. The tumor weight and photographs of the isolated tumors also demonstrated that the tumor growth was effectively suppressed in the DHM-Ce6@TPZ group under laser treatment conditions (Figure 6B and C, S11). Compared with the PBS group, all of the micelles showed no obvious side effects, evidenced by no significant difference in the mice's body weight in each treatment group throughout the course of treatment (Figure 6D). H&E staining and TUNEL staining were also used to confirm the therapeutic effect of the responsive micelles with the commercial assay kits and published protocols.[12] As shown in Figure 6E, no obvious apoptotic signs were found in tumor tissues in the PBS group. The TPZ under laser irradiation and DHM-Ce6@TPZ without light treatment significantly reduced the density of cancer cells and increased the apoptotic cells. It is worth noting that tumor tissues in the DHM-Ce6@TPZ with laser irradiation group showed the fewest cancer cells and the highest percentage of apoptosis in tumor tissues among all groups. The above results demonstrated once again that the synergistic antitumor effect of hypoxia-induced enhanced cellular uptake, hypoxia and singlet oxygen-induced rapid cargo release, and hypoxia-activated TPZ chemotherapy can be achieved using DHM-Ce6@TPZ with laser irradiation. Moreover, the H&E staining images of the main organ tissues obtained from the mice receiving different treatments showed no significant difference (Figure 7).

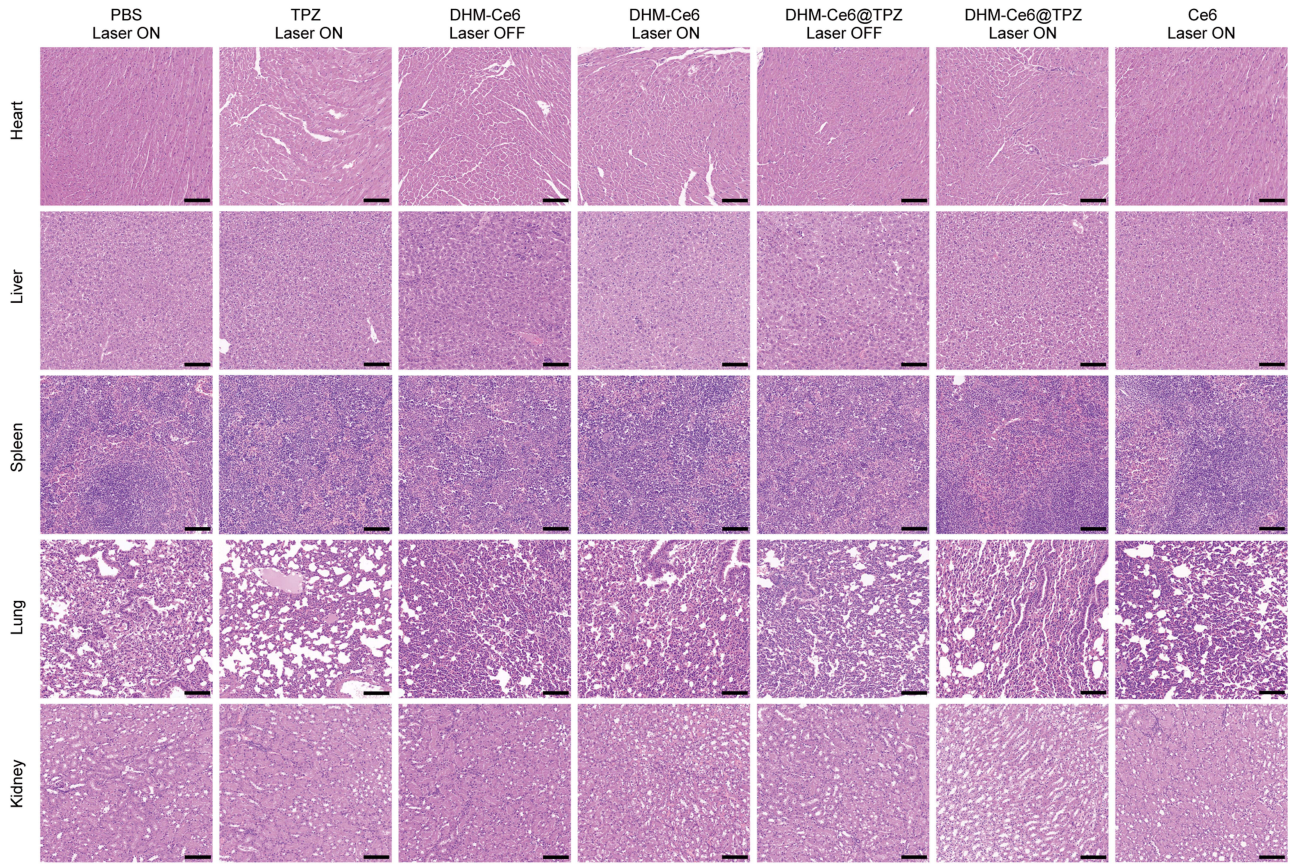

Figure 7 Histological analysis of major healthy organs (heart, liver, spleen, lung, and kidney) at the end of efficacy study (scale bar: 100 μm).

Conclusion

In summary, we designed a hypoxia- and singlet oxygen-responsive polymeric micelles containing azo and nitroimidazole groups for enhanced cellular uptake, repaid cargo release, and responsive delivery of Ce6 and TPZ, which could be used to combine Ce6-mediated PDT and PDT-activated chemotherapy to enhance the antitumor therapy effect. The hypoxia responsiveness not only increased the concentration of intracellular photosensitizer and TPZ, but also promoted Ce6 and TPZ release. Besides, under light irradiation, the nitroimidazole groups could also be oxidized to hydrophilic oxamic aldehyde by ROS, resulting in micelle disintegration and rapid cargo release. In addition, the system could reduce the oxygen level which could further enhance cellular uptake and cargo release of micelles and activation of TPZ. All in vitro and in vivo studies clearly demonstrated that the hypoxia- and singlet oxygen-responsive polymeric micelles could induce a cascade photodynamic-chemo antitumor therapy, exerting a synergistic effect on PDT and chemotherapy to inhibit tumor growth. The study integrated self-assembly, facilitated cellular uptake, stimuli-responsive disassembly, on-demand release, and interactive trigger synergism on a multifunctional micellar nano platform that could be a convenient and powerful vehicle for the efficient co-delivery of photosensitizers and chemical drugs. In addition to PDT, photothermal therapy (PTT) and chemodynamic therapy (CDT) have also attracted wide attention. PTT kills tumor cells by inducing localized hyperthermia under light irradiation. Metal ions in CDT decompose hydrogen peroxide to generate cytotoxic hydroxyl radicals that kill tumor cells. The synergistic combination of PTT, PDT and CDT is the focus of our next research.

Acknowledgments

The authors would like to thank the Natural Science Foundation of Anhui Province (2308085QH304), Key Program of Anhui University Natural Science Research (2023AH051930, 2022AH051427), and Scientific Research Projects of Bengbu Medical College of Anhui Province (2022byzd014).

Disclosure

The authors report no conflicts of interest in this work.

References

1. Khan H, Ullah H, Martorell M, et al. Flavonoids nanoparticles in cancer: treatment, prevention and clinical prospects. *Semin Cancer Biol*. 2021;69:200–211. doi:10.1016/j.semcancer.2019.07.023
2. Wicki A, Witzigmann D, Balasubramanian V, Huwyler J. Nanomedicine in cancer therapy: challenges, opportunities, and clinical applications. *J Control Release*. 2015;200:138–157. doi:10.1016/j.jconrel.2014.12.030
3. Pei Z, Chen S, Ding L, et al. Current perspectives and trend of nanomedicine in cancer: a review and bibliometric analysis. *J Control Release*. 2022;352:211–241. doi:10.1016/j.jconrel.2022.10.023
4. Ali ES, Sharker SM, Islam MT, et al. Targeting cancer cells with nanotherapeutics and nanodiagnostics: current status and future perspectives. *Semin Cancer Biol*. 2021;69:52–68. doi:10.1016/j.semcancer.2020.01.011
5. Zhi D, Yang T, O'Hagan J, Zhang S, Donnelly RF. Photothermal therapy. *J Control Release*. 2020;325:52–71. doi:10.1016/j.jconrel.2020.06.032
6. Kwiatkowski S, Knap B, Przystupski D, et al. Photodynamic therapy- mechanisms, photosensitizers and combinations. *Biomed. Pharmacother*. 2018;106:1098–1107. doi:10.1016/j.biopha.2018.07.049
7. Deng J, Liu F, Wang L, et al. Hypoxia- and singlet oxygen-responsive chemo-photodynamic micelles featured with glutathione depletion and aldehyde production. *Biomater Sci*. 2018;7(1):429–441. doi:10.1039/C8BM01042K
8. Zhong Y, Huang S, Zheng C, et al. A light and hypoxia-activated nanodrug for cascade photodynamic-chemo cancer therapy. *Biomater Sci*. 2021;9 (15):5218–5226. doi:10.1039/D1BM00660F
9. Ge L, Qiao C, Tang Y, Zhang X, Jiang X. Light-activated hypoxia-sensitive covalent organic framework for tandem-responsive drug delivery. *Nano Lett*. 2021;21(7):3218–3224. doi:10.1021/acs.nanolett.1c00488
10. Wang W, Lin L, Ma X, et al. Light-induced hypoxia-triggered living nanocarriers for synergistic cancer therapy. *ACS Appl Mater Interfaces*. 2018;10(23):19398–19407. doi:10.1021/acsami.8b03506
11. Li X, Gao M, Xin K, et al. Singlet oxygen-responsive micelles for enhanced photodynamic therapy. *J Control Release*. 2017;260:12–21. doi:10.1016/j.jconrel.2017.05.025
12. Li J, Meng X, Deng J, et al. Multifunctional micelles dually responsive to hypoxia and singlet oxygen: enhanced photodynamic therapy via interactively triggered photosensitizer delivery. *ACS Appl Mater Interfaces*. 2018;2018:1.
13. Wan Y, Fu LH, Li C, Lin J, Huang P. Conquering the hypoxia limitation for photodynamic therapy. *Adv Mater*. 2021;33(48):e2103978. doi:10.1002/adma.202103978
14. Wang D, Xue B, Ohulchanskyy TY, et al. Inhibiting tumor oxygen metabolism and simultaneously generating oxygen by intelligent upconversion nanotherapeutics for enhanced photodynamic therapy. *Biomaterials*. 2020;251:120088. doi:10.1016/j.biomaterials.2020.120088
15. Ma Y, Xu H, Sun B, et al. PH-Responsive oxygen and hydrogen peroxide self-supplying nanosystem for photodynamic and chemodynamic therapy of wound Infection. *ACS Appl Mater Interfaces*. 2021;13(50):59720–59730. doi:10.1021/acsami.1c19681
16. Zhang C, Hu X, Jin L, et al. Strategic design of conquering hypoxia in tumor for advanced photodynamic therapy. *Adv Healthc Mater*. 2023;12: e2300530. doi:10.1002/adhm.202300530
17. Guo X, Liu F, Deng J, et al. Electron-accepting micelles deplete reduced nicotinamide adenine dinucleotide phosphate and impair two antioxidant cascades for ferroptosis-induced tumor eradication. *ACS Nano*. 2020;14:14715–14730. doi:10.1021/acsnano.0c00764
18. Perche F, Biswas S, Wang T, Zhu L, Torchilin VP. Hypoxia-targeted siRNA delivery. *Angew Chem Int Ed Engl*. 2014;53(13):3362–3366. doi:10.1002/anie.201308368
19. Xu Z, Pan C, Yuan W. Light-enhanced hypoxia-responsive and azobenzene cleavage-triggered size-shrinkable micelles for synergistic photodynamic therapy and chemotherapy. *Biomater Sci*. 2020;8(12):3348–3358. doi:10.1039/D0BM00328J
20. Xu Y, Chen P, Tang L, et al. Hypoxia responsive and tumor-targeted mixed micelles for enhanced cancer therapy and real-time imaging. *Colloids Surf B Biointerfaces*. 2022;215:112526. doi:10.1016/j.colsurfb.2022.112526
21. Filipczak N, Joshi U, Attia SA, et al. Hypoxia-sensitive drug delivery to tumors. *J Control Release*. 2022;341:431–442. doi:10.1016/j.jconrel.2021.11.034
22. Li Y, Jeon J, Park JH. Hypoxia-responsive nanoparticles for tumor-targeted drug delivery. *Cancer Lett*. 2020;490:31–43. doi:10.1016/j.canlet.2020.05.032
23. Zhou Q, Mohammed F, Wang Y, et al. Hypoxia-responsive block copolymer polyprodrugs for complementary photodynamic-chemotherapy. *J Control Release*. 2021;339:130–142. doi:10.1016/j.jconrel.2021.09.023
24. Dutta D, Zhou Q, Mukerabigwi JF, Lu N, Ge Z. Hypoxia-responsive polyprodrug nanocarriers for near-Infrared light-boosted photodynamic chemotherapy. *Biomacromolecules*. 2021;22(11):4857–4870. doi:10.1021/acs.biomac.1c01152
25. Chen W, He H, Jiao P, et al. Metal-organic framework for hypoxia/ROS/pH triple-responsive cargo release. *Adv Healthc Mater*. 2023;12:e2301785. doi:10.1002/adhm.202301785
26. Yan Q, Guo X, Huang X, et al. Gated mesoporous silica nanocarriers for hypoxia-responsive cargo release. *ACS Appl Mater Interfaces*. 2019;11 (27):24377–24385. doi:10.1021/acsami.9b04142
27. Verwilst P, Han J, Lee J, et al. Reconsidering azobenzene as a component of small-molecule hypoxia-mediated cancer drugs: a theranostic case study. *Biomaterials*. 2017;115:104–114. doi:10.1016/j.biomaterials.2016.11.023
28. Zhang X, Wu M, Li J, et al. Light-enhanced hypoxia-response of conjugated polymer nanocarrier for successive synergistic photodynamic and chemo-therapy. *ACS Appl Mater Interfaces*. 2018;10:21909–21919. doi:10.1021/acsami.8b06491
29. Zhang L, Wang Z, Zhang Y, et al. Erythrocyte membrane cloaked metal-organic framework nanoparticle as biomimetic nanoreactor for starvation-activated colon cancer therapy. *ACS Nano*. 2018;12(10):10201–10211. doi:10.1021/acsnano.8b05200
30. Mahmoud AM, de Jongh P, Briere S, et al. Carboxylated Cy5-labeled comb polymers passively diffuse the cell membrane and target mitochondria. *ACS Appl Mater Interfaces*. 2019;11(34):31302–31310. doi:10.1021/acsami.9b09395
31. Matsumoto Y, Nichols JW, Toh K, et al. Vascular bursts enhance permeability of tumour blood vessels and improve nanoparticle delivery. *Nature Nanotechnol*. 2016;11(6):533–538. doi:10.1038/nnano.2015.342

32. Matsumura Y, Maeda H. A new concept for macromolecular therapeutics in cancer chemotherapy: mechanism of tumoritropic accumulation of proteins and the antitumor agent smancs. *Cancer Res*. 1986;46:6387–6392.
33. Blanco E, Shen H, Ferrari M. Principles of nanoparticle design for overcoming biological barriers to drug delivery. *Nature Biotechnol*. 2015;33(9):941–951. doi:10.1038/nbt.3330